applied sciences

MDPI

Article

Effect of Transmission Lines on the Induced Potential of Oil and Gas Pipelines Under Crossing Conditions

Jixing Sun [1,*], Qianbing Wang [1], Zhao Dong [2], Yide Liu [1], Yanhui Zhang [1] and Yuming Huo [1]

[1] School of Electrical Engineering, Beijing Jiaotong University, Haidian District, Beijing 100044, China
[2] China Power Construction Corporation Hebei Electric Power Survey and Design Institute Co., Ltd., Shijiazhuang 050031, China
* Correspondence: sanyou345@163.com; Tel.: +86-15801067328

Abstract

Railway transportation networks increasingly share constrained corridors with transmission lines, buried pipelines, and other linear infrastructure. Electromagnetic interference in these corridors is important for safe railway planning and operation, particularly when nearby high-voltage lines cross oil and gas pipelines. This paper investigates transmission-line-induced pipeline potential under crossing conditions in the Zhangbei region. The CDEGS moment-method framework is applied with locally refined segmentation in the crossing regions, and an electromagnetic coupling model for multiple-crossing transmission line-oil and gas pipeline systems is established. The qualitative effects of crossing angle and parallel length on pipeline potential were obtained under both normal operating conditions and single-phase ground fault transient conditions. The results show that induced voltage decreases nonlinearly as the crossing angle increases and rises markedly with crossing length. The contribution of ground potential rise during transient processes to pipeline potential is significantly greater than that during steady-state processes. Installing zinc ribbons as a drainage measure can reduce the pipeline-to-ground voltage. However, supplementary mitigation measures may still be required under severe interference conditions. These findings are relevant to railway transportation because railway corridors often coexist with transmission lines and buried pipelines, making coordinated electromagnetic compatibility assessment essential for infrastructure safety and operational reliability. The proposed framework supports corridor planning, risk assessment, and protective design for railway-related infrastructure in complex shared corridors.

Keywords: electromagnetic interference; pipeline potential; crossing conditions; mitigation measures

Check for updates

Academic Editors: Heinrich D. Foltz and Brent Wilson

Received: 19 May 2026
Revised: 12 June 2026
Accepted: 18 June 2026
Published: 25 June 2026

Copyright: © 2026 by the authors. Licensee MDPI, Basel, Switzerland. This article is an open access article distributed under the terms and conditions of the Creative Commons Attribution (CC BY) license.

1. Introduction

With rapid economic development, both AC transmission lines and oil/gas pipelines have expanded extensively. Owing to high population density and limited land resources, transmission lines and pipelines frequently run in parallel, cross, or even share the same right-of-way (ROW). As a consequence, electromagnetic interference (EMI) of AC transmission lines on metallic pipelines has become an increasingly prominent issue. Electrical interference from inductive, conductive, and capacitive coupling can affect pipelines collocated in close proximity to HVAC power lines, and AC interference has been a growing concern across multiple industries as improved pipeline coatings and utility ROW congestion have contributed to a rising number of identified AC corrosion incidents [1–3]. When

AC transmission lines run adjacent to oil/gas pipelines, two categories of EMI must be considered. The first is the steady-state inductive, capacitive, and conductive coupling that arises from the normal load current and operating voltage. The second is the transient EMI induced when the line is struck by lightning or experiences a single-phase-to-ground fault. A phase-to-ground fault or a lightning strike on an HVAC power line can produce large potential differences between the line and adjacent or crossing pipelines; if the potential gradient through the soil is sufficient, a direct arc to a collocated pipeline is possible, which can result in coating damage, arc damage to the pipe wall up to burn-through, and even molten pits that may trigger crack propagation. Both categories of interference can therefore endanger personnel, puncture the pipeline coating, and aggravate AC corrosion [4,5].

In 1989, Dawalibi and Southey established a mathematical model that effectively analyzed both inductive and conductive coupling, and the model has been widely applied in engineering practice owing to its convenience and accuracy [6]. New models have subsequently been developed, and existing algorithms are continuously being refined. The Electromagnetic Transient Program (EMTP) has been used by several researchers to evaluate EMI between transmission lines and pipelines under different operating states [7,8]. Christoforidis, Labridis and Dokopoulos analyzed inductive interference on pipelines buried in multilayer soil due to magnetic fields from nearby faulted power lines using a finite-element-based hybrid method [9]. Satsios, Labridis and Dokopoulos developed a hybrid algorithm combining Faraday's law of electromagnetic induction, the finite element method (FEM) and loop analysis to quantify the EMI of double-circuit lines on pipelines, with emphasis on induced voltages under asymmetric operation and fault conditions [10]. Christoforidis, Labridis and Dokopoulos further extended this hybrid FEM–circuit approach to calculate the inductive interference caused by faulted power lines on nearby buried pipelines, with particular emphasis on multi-layer soil conditions and the effect of fault current magnitude and duration on the pipeline induced voltage [11]. Czumbil, Micu et al. introduced artificial intelligence techniques (artificial neural networks and neuro-fuzzy systems) into the field–circuit coupling problem, which simplifies the modeling and shortens the computing time [12]. A distributed fuzzy logic controller scheme has been developed to address AC corrosion in pipelines exposed to electromagnetic interference from overhead transmission lines [13]. An open-source finite element framework (FLARE) has been recently proposed to model electromagnetic interference on buried metallic pipelines, offering a flexible and scalable platform for computerized mitigation studies [14]. However, such data-driven rules rely heavily on training samples, and their applicability to high-frequency transients such as lightning strikes has yet to be fully verified.

Research on algorithms suitable for engineering practice has also progressed considerably. Munteanu et al. proposed a three-dimensional coupled FEM–BEM numerical model for the electromagnetic field generated by HV overhead lines on buried pipelines, in which one-dimensional FEM pipe elements describing the pipe interior are coupled with three-dimensional BEM integral equations describing the exterior; the model was verified against the Transmission Line Method and CIGRÉ formulae, and applied to induced-potential calculations under normal and fault conditions [15]. Kopsidas and Cotton studied transient induced voltages on both aerial and buried pipelines, simulated parallelisms of up to 10 km and modeled tower–pipeline backflashovers, showing that aerial pipelines are more vulnerable to transient induced voltages, that the induced voltage saturates beyond a critical parallel length, and that backflashovers constitute an important factor in determining the maximum induced voltage [16]. Coelho, Sotelo and Lima compared two strategies for representing a pipeline—using only the section near the interfering line versus its total length—under both normal load and fault conditions, and showed that the common practice of considering only the closest region may significantly underestimate

the induced voltage [17]. A finite element analysis-based evaluation of AC interference mitigation measures for buried pipelines has been presented, demonstrating the influence of different protective configurations [18]. The coupling interference between high-voltage overhead lines and adjacent buried steel pipelines has been systematically evaluated using the CDEGS software platform [19]. In addition, Kubiczek and Kampik proposed a fast and stable method for analyzing the induced power and proximity effect under the external harmonic magnetic field for cylindrical multilayer conductors, which can provide a reference for the assessment of induced current density [20].

Zhang et al. used COMSOL Multiphysics—based on the finite element method rather than the method of moments—to analyze the interference law of AC transmission lines on the cathodic-protection potential of long-distance pipelines; their results revealed that the induced voltage is largest at the two pipeline ends and vanishes at the middle, that the potential shift increases with voltage level and decreases with parallel spacing, conductor height and pipe burial depth, and that a horizontal phase arrangement produces the largest cathodic-protection potential deviation while an umbrella arrangement produces the smallest, providing a basis for the design of buried pipelines and cathodic-protection schemes [21]. Similar common-corridor problems involving electrified railways have also been investigated: Chen et al. built a CDEGS simulation model of a single-phase AC traction supply system with a parallel buried pipeline, validated its impedance characteristics against Carson's theory and field measurements on the Baotou–Lanzhou railway/Lanzhou–Yinchuan pipeline, and analyzed the sensitivity of the induced voltage to traction-load current, load position, harmonics, parallel length, parallel spacing, coating resistivity and soil resistivity; zinc-pole drainage was installed in situ and proved effective in reducing the pipeline AC voltage below the 4 V national-standard limit [22].

Transient studies have likewise attracted considerable attention. For lightning strikes, several groups have used CDEGS-type models to analyze the coupling between the lightning transient and the pipeline. Yuan et al. combined EMTP simulation of tower and ground-wire currents with the method of moments and the Fourier transform to calculate the transient coating-stress voltage and total electric field for a pipeline parallel to, or crossing, a lightning-struck line, and derived approximate formulas for the maximum coating-stress voltage as a function of lightning current, soil resistivity and pipe–tower separation [23]. Mousa et al. modeled an underground gas pipeline running parallel to a 345-kV transmission tower struck by lightning using HIFREQ and FFTSES, determined an appropriate line-to-pipeline distance as a function of lightning current, soil properties and coating withstand voltage, and demonstrated that horizontal and vertical grounding rods can reduce the coating overvoltage [24]. Wang et al. developed a three-dimensional CDEGS simulation model that predicted the coating stress voltage of a steel pipeline in a public corridor when a typical lightning stroke impacts a tower, accounting for both first and subsequent return strokes and for resistive as well as inductive coupling, and used COMSOL to obtain the surface-potential and current-density distributions [25]. El Gayar and Abdul-Malek investigated lightning-induced voltages on a gas pipeline due to strikes on a nearby double-circuit 132-kV transmission line, considering different soil resistivities and lightning-surge waveforms, and showed that CDEGS is more accurate than circuit-based PSCAD simulations because it accounts simultaneously for multiple soil structures and for inductive, capacitive and conductive coupling [26]. Rabbani et al. analyzed the induced effects on a buried pipeline from a direct lightning strike on the ground above or near the pipe through an electromagnetic-analysis approach, quantifying the influence of soil resistivity, burial depth and strike location [27].

Based on CDEGS simulations, Dushimimana et al. analyzed the induced electromagnetic field on underground metallic pipelines running parallel to nearby HVAC power

lines, and demonstrated that the induced pipeline-to-soil voltage rises with the parallel exposure length before saturating, decreases with increasing line-to-pipeline separation, and is significantly affected by soil resistivity; they further verified that gradient-control wires provide an effective mitigation measure under fault conditions [28]. Southey, Ruan, Dawalibi and Fortin reported a parametric study of AC mitigation requirements for pipelines installed in HVAC corridors under fault conditions, demonstrating that an increase in uniform soil resistivity from 25 Ω·m to 1000 Ω·m raises the required zinc-ribbon mitigation length from less than 13 m to about 200 m, and that pipeline coating resistance, length of parallelism, structure grounding, fault-current levels, and proximity all strongly influence the mitigation requirements [29]. Christoforidis, Labridis and Dokopoulos extended FEM-based inductive-interference analysis to imperfectly coated pipelines in the presence of nearby faulted parallel lines, coupling FEM, Faraday's law and standard circuit analysis to compute induced voltages and currents at coating defects, and showed that non-parallel exposures can be handled by converting them into equivalent parallel ones [30].

Based on the method of moments and using CDEGS, the present study investigates the effects of crossing angle and crossing length between transmission lines and oil/gas pipelines on the pipeline coating voltage under different operating conditions, and examines two protective schemes—zinc-ribbon drainage and dedicated grounding devices—through quantitative simulation.

2. Crossing Model for Overhead Transmission Lines and Oil and Gas Pipelines

Oil and gas pipelines are typically installed underground. The crossing configuration with overhead transmission lines is illustrated in Figure 1, showing both parallel and crossing arrangements between oil and gas pipelines and transmission lines.

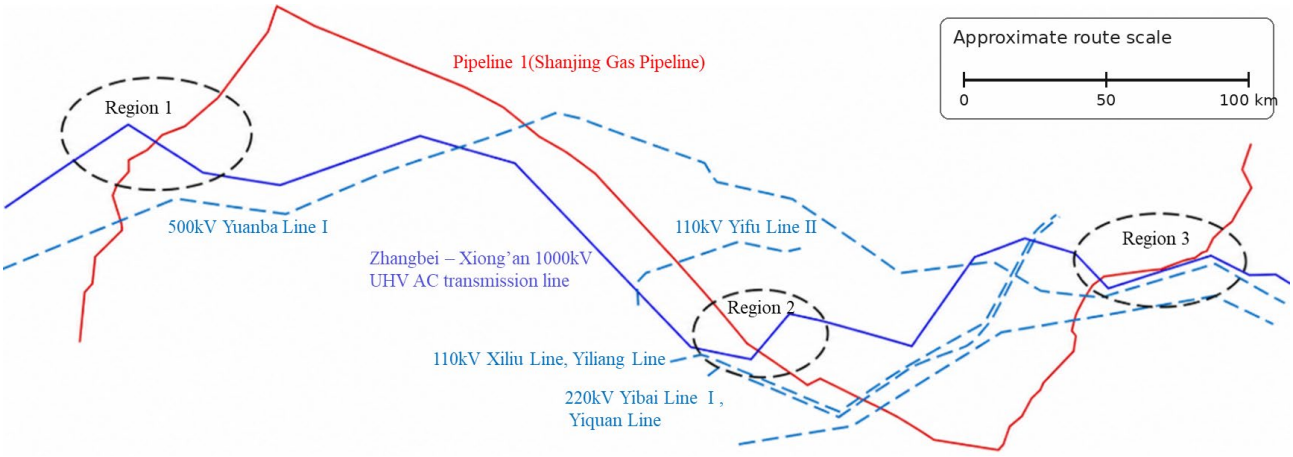


Figure 1. Crossing configurations between gas pipelines and power lines.

2.1. Electromagnetic Interference Model for Crossing Lines

Based on distributed-source transmission line theory, the electromagnetic influence of high-voltage transmission lines on adjacent oil and gas pipelines is studied [31]. The earth is treated as a reference conductor, and each pipe segment is treated as a differential element. An equivalent oil and gas pipeline–earth return transmission line model is established, as shown in Figure 2.

Using the pipeline-earth equivalent circuit, the frequency-domain equations are:

$$\frac{dU(x)}{dx} + ZI(x) - E(x) = 0 \quad (1)$$

$$\frac{dI(x)}{dx} + YU(x) = 0 \tag{2}$$

where U and I are the induced voltage and current along the pipeline; Z and Y are the series impedance and shunt admittance per unit length of the pipeline–earth return; and E is the induced electromotive force per unit length of the pipeline.

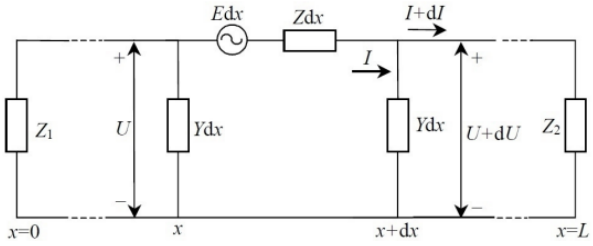


Figure 2. Pipeline-earth return transmission line model.

Combining Equations (1) and (2) yields:

$$\frac{d^2U(x)}{dx^2} - ZYU(x) - \frac{\mathrm{d}E(x)}{dx} = 0 \tag{3}$$

$$\frac{d^2I(x)}{dx^2} - ZYI(x) + YE(x) = 0 \tag{4}$$

Assuming E is constant on the differential element, the general solution takes the form:

$$U(x) = Ae^{\gamma x} + Be^{-\gamma x} \tag{5}$$

where γ is the propagation constant, $\gamma = \sqrt{\mathrm{ZY}}$; and Z_c is the characteristic impedance, $Z_c = \sqrt{\mathrm{Z/Y}}$.

Combining Equations (1) and (5) yields:

$$I(x) = \frac{E}{Z} - \frac{1}{Z_c}(Ae^{\gamma x} - Be^{-\gamma x}) \tag{6}$$

Applying the terminal boundary conditions $U(L) = Z_2I(L)$ and $U(0) = -Z_1I(0)$, the solutions are

$$A = \frac{E[(1+\rho_1)\rho_2 - (1+\rho_2)e^{\gamma L}]}{2\gamma(\rho_1\rho_2 - e^{2\gamma L})} \tag{7}$$

$$B = \frac{E[(1+\rho_1)e^{2\gamma L} - \rho_1(1+\rho_2)e^{\gamma L}]}{2\gamma(\rho_1\rho_2 - e^{2\gamma L})} \tag{8}$$

where

$$\rho_1 = \frac{Z_1 - Z_C}{Z_1 + Z_C} \tag{9}$$

$$\rho_2 = \frac{Z_2 - Z_C}{Z_2 + Z_C} \tag{10}$$

In practical engineering, the pipeline extends infinitely at both ends after running parallel to the line for a certain distance. In this paper, $Z_1 = Z_2 = Z_c$ is adopted.

2.2. Leakage Current Calculation Using the Moment Method

The moment method is the built-in algorithm of the CDEGS software. Its core principle is to discretize conductors into a number of segments. Let the midpoint of the k-th conductor segment be k, with endpoints k^+ and k^-. The corresponding endpoint currents are I^l_{k+} and

$I_{k^-}^l$, and the current in the p-th conductor segment is I_p^n. The self-impedance Z_{kp} of the p-th segment in the k-th conductor segment is:

$$Z_{kp} = \frac{\rho}{4\pi l_p}\int [\frac{1}{\sqrt{r_{kp}^2 + z_{kp}^2}} + \sum_{i=1}^{N} (\frac{a_i}{\sqrt{r_{kp}^2 + (z_{kp}^2 - b_i)^2}} + \frac{c_i}{\sqrt{r_{kp}^2 + (z_{kp}^2 + d_i)^2}})]d \quad (11)$$

where a_i and c_i are the magnitudes of the image sources, and b_i and d_i are their positions.

The scalar potential φ_k generated by the leakage current of the k-th conductor segment is:

$$\phi_k = \sum_{P=1}^{K} Z_K I_N^P (k = 1, 2, \ldots, K) \quad (12)$$

The leakage current I_k^n of the k-th conductor segment is:

$$I_n^k = I_{k^-}^l - I_{k^{+-}}^l \quad (13)$$

The leakage current of each conductor segment is expressed as:

$$I_k^s = \sum_{p=1}^{K} a_{kp} I_p^n \quad (14)$$

Since $I_k^s = 0$, the leakage current I_k^n of each conductor segment is obtained by solving the resulting linear system of equations, which ultimately yields the leakage current distribution over the entire conductor.

Compared with the traditional FEM and fuzzy algorithms, this method ensures computational efficiency while being more suitable for complex conditions such as multiple crossings and long-distance parallel arrangements. In this paper, the moment method is applied with refined segmentation in the crossing region to improve the accuracy of local current density calculations. The image source coefficients are adjusted based on measured resistivity data from the Zhangbei region.

2.3. Crossing Conditions and Simulation

The electromagnetic interference model between transmission lines and oil and gas pipelines is primarily governed by soil parameters and the spatial relative positions of the two systems. A schematic diagram of a typical interference model is shown in Figure 3. Here, L_1 is defined as the total length of the transmission line in the pipeline–line crossing model, L_2 represents the length of the crossing section between the pipeline and the transmission line, and L_3 represents the length of the pipeline sections at both ends extending to the far end (at 90° to the transmission line). The specific crossing angle and crossing length are adjusted according to the analyses in subsequent sections. Model parameters are set as shown in Table 1.

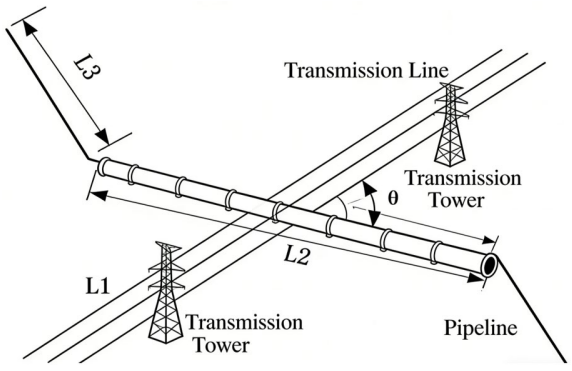


Figure 3. Schematic diagram of relative positions in the electromagnetic interference model.

Table 1. Model parameters.

Line Parameters		Pipe Parameters	
Phase Line (JL1/LHA1)	Relative Resistivity: 1.5 Relative Permeability: 1	Inner Diameter Outer Diameter	640 mm 660 mm
Phase Sequence	ABC-CBA	Burial Depth	1.9 m
Shield Wire (OPGW-185)	Relative Resistivity: 3.3 Relative Permeability: 1	Pipe Metal	Relative Resistivity: 10 Relative Permeability: 300
Tower Grounding Device (TJ20)	Burial Depth: 0.8 m Side Length: 18 m	Anti-corrosion Coating (3PE)	Thickness: 3 mm Resistivity: 105

Considering the typical characteristics of power line construction and soil grounding conditions in the Zhangbei region, a 1000 kV transmission line typical of this area was used for basic modeling and analysis. The cross-sectional layout of the conductors and shield wires is shown in Figure 4. The section of the transmission line crossing the pipeline is a 1000 kV double-circuit same-tower line with a drum-type tower configuration and a span of 500 m.

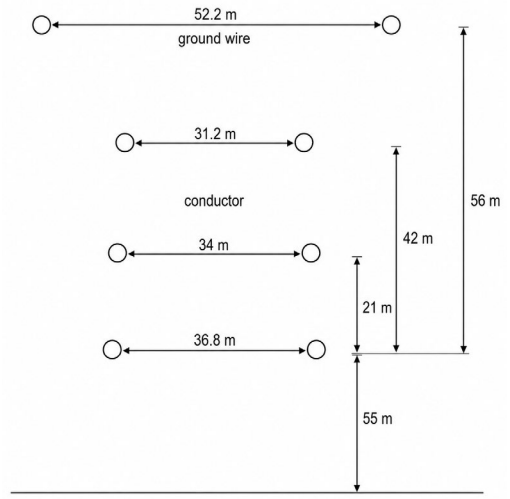


Figure 4. Cross-section of conductors and shield wires.

The transmission capacity is 5300 MW. During normal double-circuit operation, the line current is 1530 A. When a single-phase ground fault occurs, the fault current entering the ground is 21,400 A. Typical line and pipeline parameters are listed in Table 1.

Referring to the measured soil resistivity values at typical pipeline crossings in the Zhangbei region, a shallow-layer soil resistivity of 30 Ω·m is used when calculating the AC corrosion pipeline-to-ground voltage during double-circuit line operation. A deep-layer soil resistivity of 241 Ω·m at 10 m depth is used when calculating the pipeline interference voltage during a single-phase short-circuit fault. Figure 1 shows the crossing route map of the Shaanxi–Beijing gas pipeline and the adjacent AC transmission lines in the Zhangbei region. An electromagnetic interference model was established for multiple conditions, including crossings and parallel runs between the Shaanxi–Beijing gas pipeline and the 1000 kV AC transmission line in this region. The pipeline–line crossing point nearest to Zhangbei Station is approximately 260 km from the station, with three crossings occurring at angles of 81°, 88°, and 75°, and crossing section lengths of 1.2 km, 0.8 km, and 1.5 km, respectively. Considering the height difference between the tower grounding devices and the pipeline, the minimum distances from the pipeline to the centers of the tower grounding devices are approximately 167.4 m, 147.4 m, and 35.5 m, respectively. Based on these conditions, an electromagnetic interference model was established for multiple

conditions, including crossings and parallel runs between the Shaanxi–Beijing gas pipeline and the 1000 kV AC transmission line. The coordinate origin is selected at the crossing point that is closest to the Zhangbei substation, the positive direction of the x-axis is the main direction along the pipeline in the horizontal plane, and the y-axis represents the lateral relative position between the transmission line and the pipeline, as shown in Figure 5.

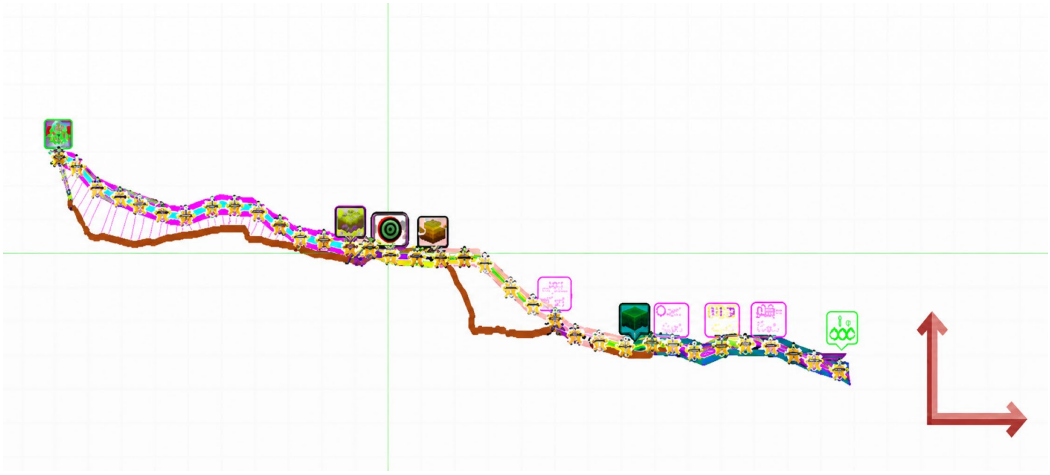


Figure 5. Electromagnetic interference model under multiple conditions, including crossings and parallel runs.

3. Numerical Analysis of Pipeline-to-Ground Potential Under Crossing Conditions

3.1. Electromagnetic Interference Analysis Under Single-Crossing Conditions

The crossing angle, crossing length, transient process, and steady-state process all influence the shell potential of the pipeline. As shown in Figure 6, during normal double-circuit operation of the 1000 kV UHV AC transmission line, the maximum pipeline-to-ground voltage on pipeline 1 is 9.2 V, and the maximum leakage current density is 68.9 A/m^2. The peak values of the pipeline-to-ground voltage appear at the three crossing regions shown in Figure 5. According to the provisions of GB/T 50698-2011 "Technical Standard for AC Interference Mitigation of Buried Steel Pipelines," pipelines with an AC leakage current density exceeding 30 A/m^2 must adopt AC interference protection measures [32].

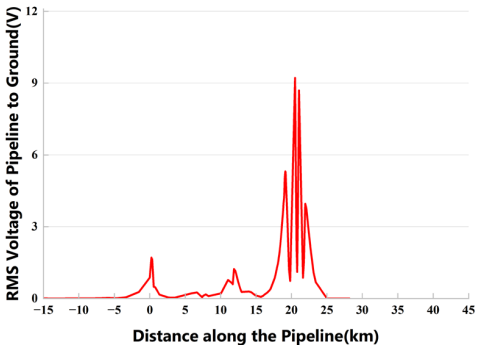


Figure 6. Simulation results of pipeline-to-ground voltage distribution along pipeline 1 during double-circuit operation of the 1000 kV UHV AC transmission line in the Zhangbei region.

3.2. Electromagnetic Interference Analysis Under Multiple-Crossing Conditions

In the vicinity of the section where pipeline 1 approaches the transmission line of this project, other AC transmission lines at voltage levels of 110 kV and above are present. The relative positional relationships between these adjacent lines and the pipeline are shown in

Figure 5. Table 2 lists the names and transmission currents of adjacent AC lines provided by the design unit.

Table 2. Transmission current parameters of adjacent AC lines.

Line Name	Single-Circuit Transmission Current (A)	Line Construction Method
500 kV Yuanba Line I	1200	Single circuit line
500 kV Yuanba Line II	1200	Single circuit line
220 kV Yibai Line, Yiquan Line	40	Double circuit line
110 kV Yifu Line II	40	Single circuit line
110 kV Xiliu Line	60	Single circuit line
110 kV Yiliang Line	250	Single circuit line

Following the same calculation procedure as in Section 3.1, individual models were established for the influence of each AC transmission line at 110 kV and above on adjacent pipeline 1. The pipeline-to-ground voltages induced during normal operation were calculated, and the results were combined using the root-sum-square (RSS) method to represent the comprehensive influence of all AC transmission lines on the pipeline. In this paper, RSS is used only as an initial estimate of the comprehensive influence of multiple lines. When synchronized phasor data are available, phasor superposition should be used instead. Figure 7a,b show the distributions of pipeline-to-ground voltage along pipeline 1 induced by individual transmission lines. Figure 7c shows the distribution of the combined pipeline-to-ground voltage considering all AC transmission lines at 110 kV and above. Table 3 lists the maximum pipeline-to-ground voltage and the corresponding maximum AC leakage current density that may be produced on pipeline 1 by each AC transmission line at 110 kV and above. From Figure 7c and Table 3, the maximum pipeline-to-ground voltage on pipeline 1 during double-circuit operation is 9.9 V, the maximum leakage current density is 75 A/m^2, and the most severely interfered region is concentrated in crossing zone 3 shown in Figure 1.

Table 3. Results of the comprehensive impact on pipelines during normal operation of 110 kV and higher AC transmission lines.

Transmission Line Name	Maximum Pipeline-to-Ground Voltage (V)	AC Current Density (mA/cm^2)
Zhangbei-Xiong'an 1000 kV UHV AC Transmission Line	9.2	7.5
500 kV Yuanba Line I	3.0	
220 kV Yibai Line, Yiquan Line	<0.1	
110 kV Yifu Line II	<0.1	
110 kV Xiliu Line	<0.1	
110 kV Yiliang Line	0.3	
Overall results	9.9	

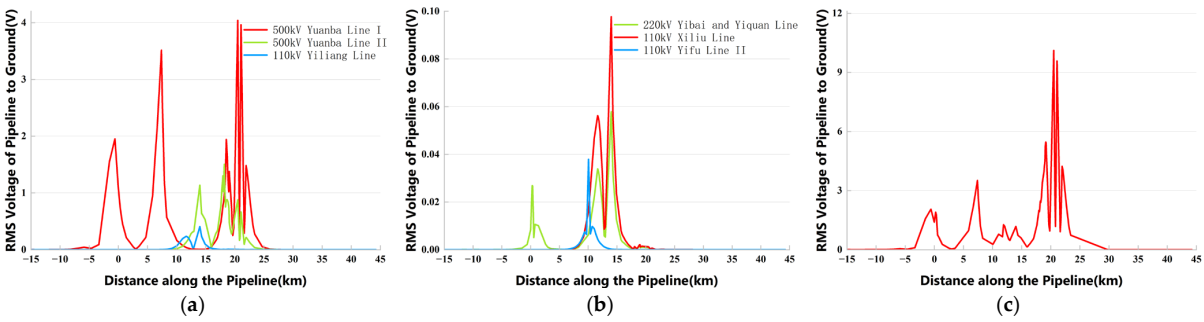


Figure 7. (**a**) Simulation results 1 of pipeline-to-ground voltage from individual transmission lines; (**b**) simulation results 2 of pipeline-to-ground voltage from individual transmission lines; (**c**) simulation results of combined pipeline-to-ground voltage from all transmission lines.

4. Effect of Crossing Parameters on Electromagnetic Interference Characteristics

4.1. Effect of Crossing Angle on Pipeline-to-Ground Potential

4.1.1. Steady-State Analysis

To analyze the effect of crossing angle on electromagnetic interference independently, the transmission line length L_1 was set to 10 km and the pipeline crossing length was set to 5 km. Other parameters were kept unchanged. The angle θ between the transmission line and the oil and gas pipeline was varied from 15° to 90° for simulation. The results are shown in Figure 8a.

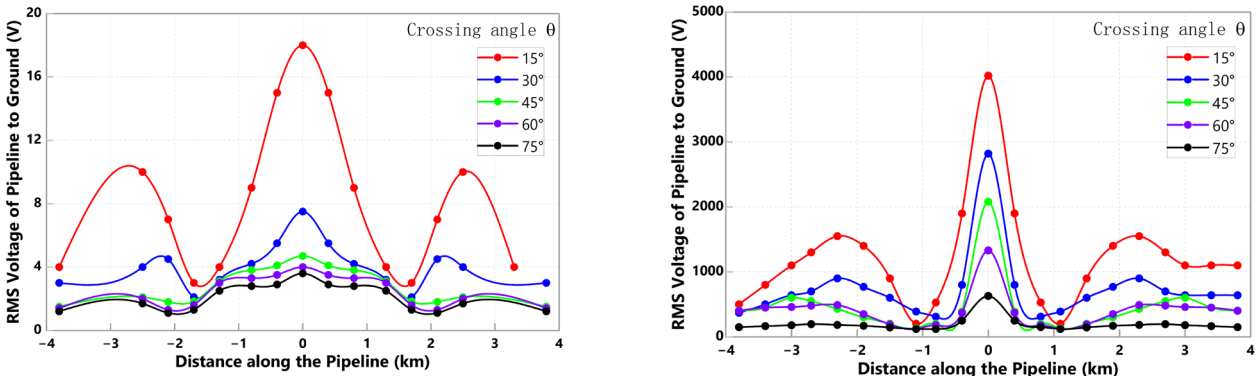


Figure 8. Simulation results for the effect of crossing angle on pipeline-to-ground potential: (**a**) normal line operation; (**b**) single-phase ground short-circuit fault.

As shown in Figure 8a, the pipeline-to-ground voltage is greatest at the crossing point. The overall variation trend of the induced voltage along the pipeline is as follows: before reaching the perpendicular sections at both ends, the pipeline-to-ground voltage first decreases rapidly and then increases slowly to a certain value. After the pipeline exits the shared corridor, the pipeline-to-ground voltage decreases rapidly again, and the electromagnetic interference weakens. In the longitudinal comparison, as the crossing angle θ increases, the pipeline induced voltage decreases markedly, from 17 V to 3.8 V. This is because the mechanism by which the transmission line generates interference voltage on the pipeline during normal operation is inductive coupling. The pipeline is treated as a long conductor cutting through the alternating magnetic field generated by the transmission line, thereby inducing a voltage. The magnitude of the induced voltage is related to the equivalent length of the pipeline portion running parallel to the transmission line. As θ increases from 0° to 75°, the equivalent parallel length decreases to nearly zero. These results confirm that a smaller crossing angle between the pipeline and the transmission line leads to more significant electromagnetic interference.

4.1.2. Effect of Single-Phase Ground Short Circuit on Pipeline-to-Ground Potential

As shown in Figure 8b, the variation trend of the pipeline-to-ground potential during a single-phase ground short circuit is nearly identical to that under steady-state conditions. Each curve represents the maximum envelope line of the impact caused by setting a single-phase grounding fault along the transmission line. The peak value still appears at the crossing point. As the crossing angle θ increases, the pipeline induced voltage decreases significantly, from 4050 V to 630 V.

4.2. Effect of Crossing Length on Pipeline-to-Ground Potential

4.2.1. Steady-State Analysis

To analyze the effect of the crossing section length on electromagnetic interference independently, other parameters were kept unchanged. The crossing angle was set to $\theta = 15°$, which produced the maximum induced potential in the test described in Section 4.1.1. The crossing length L2 was set to 1 km, 3 km, 5 km, 7 km, and 9 km for simulation. The results are shown in Figure 9.

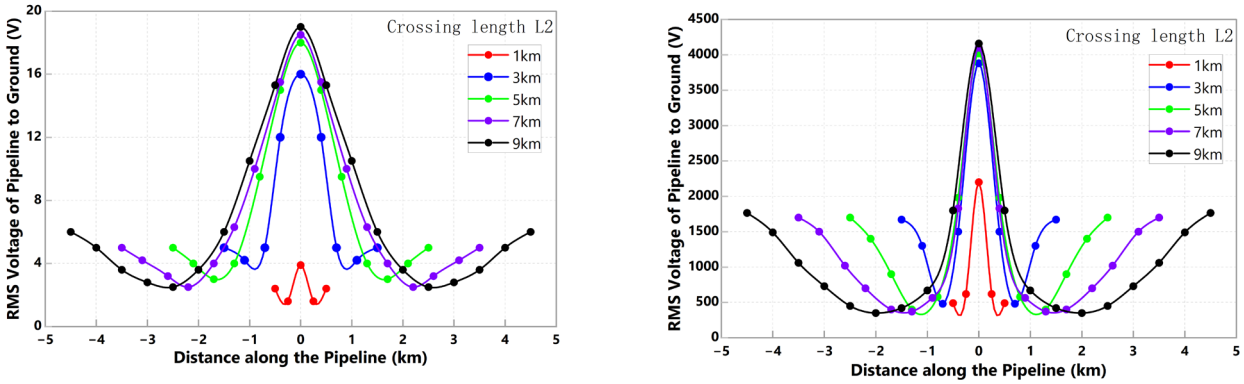


Figure 9. Simulation results for the effect of crossing length on pipeline-to-ground potential: (**a**) normal line operation; (**b**) single-phase ground short-circuit fault.

As shown in Figure 9a, the pipeline-to-ground voltage is greatest at the crossing point. The overall variation trend of the induced voltage along the pipeline is as follows: the voltage peak still appears at the crossing point, followed by a rapid attenuation and then a slow recovery along the pipeline axis. After the pipeline exits the shared corridor with the transmission line, the pipeline-to-ground voltage amplitude decays rapidly. Quantitative analysis shows that as L_2 increases from 1 km to 9 km, the maximum pipeline-to-ground potential increases monotonically from 3.9 V to 17 V, indicating a significant positive correlation between crossing section length and induced voltage intensity. This phenomenon can be explained from the perspective of electromagnetic coupling theory: the extended crossing section lengthens the action path of both inductive and resistive coupling, leading to enhanced cumulative interference. Therefore, long-distance routing of pipelines alongside transmission lines should be avoided during pipeline construction.

4.2.2. Effect of Single-Phase Ground Short Circuit on Pipeline-to-Ground Potential

As shown in Figure 9b, the variation trend of the pipeline-to-ground potential during a single-phase ground short circuit is nearly identical to that under steady-state conditions. The peak value still appears at the crossing point. As the crossing length increases, the pipeline-induced voltage increases markedly, from 2200 V to 4200 V.

5. Methods for Suppressing Induced Potential in Oil and Gas Pipelines

The limits of electromagnetic influence of high-voltage transmission line projects on oil and gas pipelines are listed in Table 4. The reference standard for the AC corrosion limit during normal line operation is GB 6830-1986 [33], and the reference standard for the personal safety limit is GB/T 50698-2011 [32]. Under single-phase ground fault conditions, the reference standard for the personal safety limit is DL/T 5033-2006 [34], and the reference standard for the safety limit of 3-layer PE (polyethylene) pipeline coating is GB/T 23257-2017 [35].

Table 4. Limits of electromagnetic influence of high-voltage transmission lines on pipelines.

Transmission Line Operating Condition	Electromagnetic Impact	Limit Values
Normal Operation	Personal Safety	60 V
	AC Corrosion of Pipeline	Pipeline-to-Soil Potential $\leq$ 4 V, OR AC Current Density < 3 mA/cm^2 when Pipeline-to-Soil Potential > 4 V
Fault Condition	Personal Safety	1500 V
	Pipeline Coating Integrity	3PE: 57 kV

Comparing all pipeline-to-ground voltages in Figures 8 and 9 with the relevant limits, it is concluded that protective measures are required for crossing angles below 60° under both steady-state and transient conditions, and that protective measures are required for all crossing lengths considered in this study.

From Figure 9a,b, the maximum pipeline-to-ground voltages for crossing lengths of 5–9 km are nearly identical under both steady-state and transient conditions. Since the variation with crossing angle is very pronounced, crossing lengths of 5 km with crossing angles of 15° and 45° were selected for the evaluation of protective measures. Appropriate installation positions for zinc ribbon drainage were identified, and the suppression effects were studied.

A commonly adopted protective measure in China's pipeline industry is to lay zinc ribbons along the pipeline. The zinc ribbons are connected to the pipeline through solid-state decouplers that block DC current while conducting AC current. This measure not only exploits the shielding effect of zinc ribbons but also effectively connects the pipeline to the ground through a low resistance due to the good grounding performance of zinc, thereby significantly reducing the pipeline-to-ground voltage.

In the simulation, zinc ribbons were symmetrically laid along the pipeline with the crossing point as the origin. The cross-sectional dimensions of the zinc ribbon were 15.88 mm × 22.22 mm, with an equivalent radius of approximately 6 mm and a burial depth of 0.8 m.

5.1. Under Steady-State Conditions

As shown in Figure 10, when zinc ribbons are laid along the pipeline at a crossing angle of θ = 15°, the peak induced voltage decreases from 17 V to 9.5 V, a reduction of 44%. Although this does not bring the voltage below the 4 V AC corrosion limit, the drainage effect is significant. At a crossing angle of θ = 45°, the peak induced voltage decreases from 4.7 V to 3.1 V, a reduction of 34%, which satisfies the limit requirement. The difference in drainage efficiency indicates that the effectiveness of zinc ribbons is closely related to the geometric configuration of the transmission line–pipeline system. A smaller crossing angle produces stronger electromagnetic coupling, making it difficult for a single drainage measure to fully eliminate the interference risk. The simulation results provide a theoretical basis for optimizing drainage systems in engineering practice. In particular, for large-angle crossings, zinc ribbon drainage can serve as an effective interference suppression measure. For small-angle crossings or long parallel sections with strong interference, multi-stage drainage or supplementary protective measures should be considered to ensure safe pipeline operation.

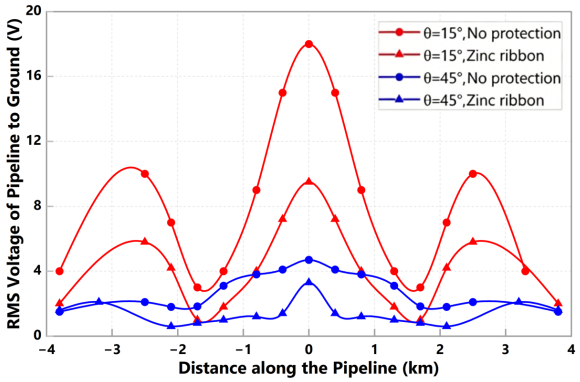


Figure 10. Simulation results for the drainage effect of zinc ribbons laid along the pipeline under steady-state conditions.

5.2. Under Transient Conditions

The distribution of short-circuit current at different positions along the line when a typical single-phase ground short-circuit fault occurs on the 1000 kV Zhangbei–Xiong'an UHV AC transmission line in the Zhangbei region is shown in Figure 11.

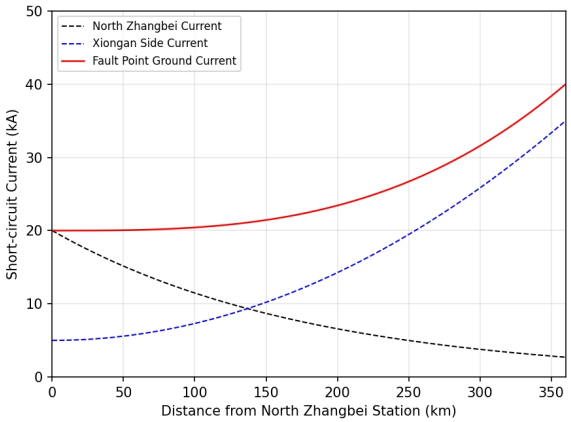


Figure 11. Distribution of fault current during a single-phase ground short circuit on the 1000 kV line in the Zhangbei region.

As shown in Figure 12, when zinc ribbons are laid along the pipeline at $\theta = 15°$, the peak induced voltage decreases from 4085 V to 3430 V, a reduction of 15%. At $\theta = 45°$, the peak induced voltage decreases from 2050 V to 1820 V, a reduction of 11%. The drainage effect is notable in both cases. However, the voltage has not yet been reduced to the personal safety limit of 1.5 kV, and the feasibility of combining this approach with other drainage measures should be further considered.

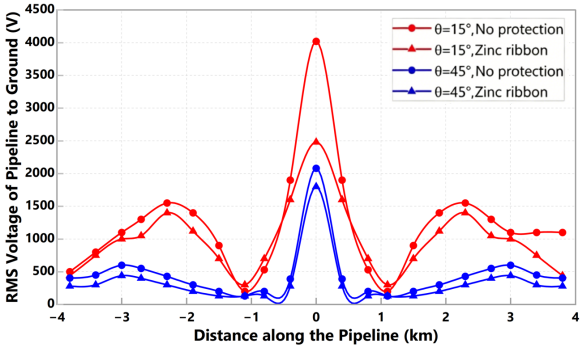


Figure 12. Simulation results for the drainage effect of zinc ribbons laid along the pipeline during a ground short circuit.

5.3. Validation Scope and Future Field-Measurement Plan

Figures 6–12 present numerical calculation results. In the present study, engineering data are used to define the model geometry and input parameters, but a dedicated measurement campaign was not available for point-by-point validation. This limitation should be considered when applying the calculated voltage envelopes to other corridors.

A future field-validation campaign should include synchronized recordings of transmission-line currents and phase angles, pipeline-to-soil AC voltages at existing test posts and temporary measurement stations near the crossing regions, AC current density measured using coupons or probes, and depth-dependent soil-resistivity surveys. Before-and-after measurements should also be conducted where zinc ribbons are installed. For fault or transient conditions, validation may use recorded disturbance events or scaled controlled experiments. The comparison should evaluate peak voltage, spatial voltage profiles, and mitigation ratios.

6. Conclusions

This paper investigated the electromagnetic interference of transmission lines on oil and gas pipelines under crossing conditions. A multi-crossing coupling model based on the moment-method was established. Based on the actual engineering parameters of the Zhangbei region, the quantitative effects of crossing angle and crossing length on pipeline potential were revealed, and the effectiveness of protective measures was verified. The main conclusions are as follows:

(1) An electromagnetic coupling model applicable to multiple-crossing conditions was established. By the CDEGS moment-method segmentation strategy and dynamically correcting soil parameters, the calculation accuracy was significantly improved, addressing the inadequate adaptability of traditional algorithms to complex crossing scenarios.

(2) When a transmission line and a pipeline cross, the peak pipeline-to-ground potential appears at the crossing point. Due to electromagnetic induction, the pipeline-to-ground potential first decreases and then increases before reaching the sections perpendicular to the line at both ends. As the pipeline exits the shared corridor, the pipeline-to-ground voltage decreases rapidly.

(3) Under both steady-state and transient operating conditions, a smaller crossing angle and a longer crossing length between the pipeline and the transmission line result in more significant electromagnetic interference and a larger induced potential. In this study, when the pipeline crossing section is 5 km, protective measures are required for crossing angles below 60°. When the crossing angle is 15°, protective measures are required regardless of the crossing length.

(4) Symmetrically laid zinc ribbons connected through solid-state decouplers effectively reduce the pipeline-to-ground voltage under both steady-state and fault conditions. However, a single zinc-ribbon drainage measure does not always reduce the voltage below the personal-safety limits under strong-interference scenarios, and supplementary mitigation measures are required in such cases.

The results of this study provide quantitative evidence and protective optimization methods for the electromagnetic compatibility design of pipelines in crossing line areas, and are particularly applicable to the parallel planning of UHV transmission lines and long-distance pipelines.

Author Contributions: Conceptualization, J.S. and Q.W.; Methodology, Z.D.; Software, Y.L.; Validation, Y.Z.; Formal Analysis, Y.H.; Investigation, J.S.; Resources, Z.D.; Data Curation, Q.W.; Writing—Original Draft Preparation, J.S. and Q.W.; Writing—Review and Editing, J.S. and Q.W.; Visualization, Y.Z.; Supervision, J.S.; Project Administration, Z.D.; Funding Acquisition, J.S., Q.W. and Z.D. All authors have read and agreed to the published version of the manuscript.

Funding: This research was funded by the National Natural Science Foundation of China (52377131).

Institutional Review Board Statement: Not applicable.

Informed Consent Statement: Not applicable.

Data Availability Statement: Data are contained within the article.

Acknowledgments: The authors would like to thank reviewers for their pertinent comments that helped improve the quality of this paper.

Conflicts of Interest: The author Zhao Dong was employed by the company China Power Construction Corporation Hebei Electric Power Survey and Design Institute Co., Ltd. The remaining authors declare that the research was conducted in the absence of any commercial or financial relationships that could be construed as a potential conflict of interest.

References

1. Martins-Britto, A.G.; Moraes, C.M.; Lopes, F.V. Inductive Interferences between a 500 kV Power Line and a Pipeline with a Complex Approximation Layout and Multilayered Soil. *Electr. Power Syst. Res.* **2021**, *196*, 107265. [CrossRef]
2. Martins-Britto, A.G.; Moraes, C.M.; Lopes, F.V. Transient Electromagnetic Interferences between a Power Line and a Pipeline Due to a Lightning Discharge: An EMTP-Based Approach. *Electr. Power Syst. Res.* **2021**, *197*, 107321. [CrossRef]
3. Cristofolini, A.; Popoli, A.; Sandrolini, L.; Pierotti, G.; Simonazzi, M. Laplace Transform for Finite Element Analysis of Electromagnetic Interferences in Underground Metallic Structures. *Appl. Sci.* **2022**, *12*, 872. [CrossRef]
4. Ouadah, M.; Touhami, O.; Ibtiouen, R.; Benlamnouar, M.F.; Zergoug, M. Corrosive Effects of the Electromagnetic Induction Caused by the High Voltage Power Lines on Buried X70 Steel Pipelines. *Int. J. Electr. Power Energy Syst.* **2017**, *91*, 34–41. [CrossRef]
5. Gouda, O.E.; Al-Gabalawy, M.A. Overhead Transmission Lines Impacts on Neighboring Buried Metallic Gas Pipelines. *Electr. Eng.* **2021**, *103*, 3119–3137. [CrossRef]
6. Dawalibi, F.P.; Southey, R.D. Analysis of Electrical Interference from Power Lines to Gas Pipelines. I. Computation Methods. *IEEE Trans. Power Deliv.* **1989**, *4*, 1840–1846. [CrossRef]
7. Wu, X.; Zhang, H.; Karady, G.G. Transient Analysis of Inductive Induced Voltage between Power Line and Nearby Pipeline. *Int. J. Electr. Power Energy Syst.* **2017**, *84*, 47–54. [CrossRef]
8. Ahmet, N. Simulation of Transient Processes on Overvoltage in Electric Transmission Lines Using ATP-EMTP. *Turk. J. Electr. Eng. Comput. Sci.* **2013**, *21*, 1553–1566. [CrossRef]
9. Christoforidis, G.C.; Labridis, D.P.; Dokopoulos, P.S. Inductive Interference on Pipelines Buried in Multilayer Soil Due to Magnetic Fields from Nearby Faulted Power Lines. *IEEE Trans. Electromagn. Compat.* **2005**, *47*, 254–262. [CrossRef]
10. Satsios, K.J.; Labridis, D.P.; Dokopoulos, P.S. Currents and Voltages Induced during Earth Faults in a System Consisting of a Transmission Line and a Parellel Pipeline. *Eur. Trans. Electr. Power* **1998**, *8*, 193–199. [CrossRef]
11. Christoforidis, G.C.; Labridis, D.P.; Dokopoulos, P.S. A Hybrid Method for Calculating the Inductive Interference Caused by Faulted Power Lines to Nearby Buried Pipelines. *IEEE Trans. Power Deliv.* **2005**, *20*, 1465–1473. [CrossRef]
12. Czumbil, L.; Micu, D.D.; Ceclan, A. Artificial Intelligence Techniques Applied to Electromagnetic Interference Problems. *IFMBE Proc.* **2009**, *26*, 339–344. [CrossRef]
13. Al-Gabalawy, M.; Mostafa, M.A.; Hamza, A.S. Design of Distributed Fuzzy Logic Controllers for Controlling the AC Corrosion in the Metallic Pipelines Due to the OHTLs. *Egypt. J. Pet.* **2020**, *29*, 235–241. [CrossRef]
14. Popoli, A.; Pierotti, G.; Ragazzi, F.; Sandrolini, L.; Cristofolini, A. FLARE: A Framework for the Finite Element Simulation of Electromagnetic Interference on Buried Metallic Pipelines. *Appl. Sci.* **2023**, *13*, 6268. [CrossRef]
15. Munteanu, C.; Mates, G.; Purcar, M.; Topa, V.; Pop, I.T.; Grindei, L.; Racasan, A. Electromagnetic Field Model for the Numerical Computation of Voltages Induced on Buried Pipelines by High Voltage Overhead Power Lines. *Eur. Phys. J. Appl. Phys.* **2012**, *58*, 30902. [CrossRef]
16. Kopsidas, K.; Cotton, I. Induced Voltages on Long Aerial and Buried Pipelines Due to Transmission Line Transients. *IEEE Trans. Power Deliv.* **2008**, *23*, 1535–1543. [CrossRef]
17. Coelho, L.; Sotelo, G.; Lima, A.C.S. Detailed versus Simplified Representation of a Pipeline for Assessment of Inductive and Conductive Couplings to an Overhead Transmission Lines during Steady-State and Fault Conditions. *Int. J. Electr. Power Energy Syst.* **2022**, *142*, 108350. [CrossRef]
18. Popoli, A.; Sandrolini, L.; Cristofolini, A. Finite Element Analysis of Mitigation Measures for AC Interference on Buried Pipelines. In Proceedings of the 2019 IEEE International Conference on Environment and Electrical Engineering and 2019 IEEE Industrial and Commercial Power Systems Europe (EEEIC/I&CPS Europe), Genova, Italy, 11–14 June 2019. [CrossRef]

19. Wang, X.; Wang, Y.; Sun, T.; Yang, X.; Yang, L.; Qi, Y. Study of the Coupling Interference of High-Voltage Transmission Lines on Adjacent Buried Steel Pipelines Based on CDEGS. *Electr. Power Syst. Res.* **2023**, *217*, 109125. [CrossRef]
20. Kubiczek, K.; Kampik, M. Fast and Numerically Stable Analytical Computations for the Power Induced in Cylindrical Multilayered Conductors Under External Magnetic Fields. *IEEE Trans. Electromagn. Compat.* **2023**, *65*, 292–299. [CrossRef]
21. Zhang, B.; Li, L.; Zhang, Y.; Wang, J. Study on the Interference Law of AC Transmission Lines on the Cathodic Protection Potential of Long-Distance Transmission Pipelines. *Magnetochemistry* **2023**, *9*, 75. [CrossRef]
22. Chen, M.; Liu, S.; Zhu, J.; Xie, C.; Tian, H.; Li, J. Effects and Characteristics of AC Interference on Parallel Underground Pipelines Caused by an AC Electrified Railway. *Energies* **2018**, *11*, 2255. [CrossRef]
23. Yuan, H.; Qi, L.; Wu, Y.; Cui, X.; Wang, L. Lightning Induced Voltage on the Underground Pipeline near Overhead Transmission Line. In Proceedings of the 2011 7th Asia-Pacific International Conference on Lightning (APL), Chengdu, China, 1–4 November 2011; pp. 411–415. [CrossRef]
24. Mousa, M.I.; Abdul-Malek, Z.; Ibrahim, V.M.; Elgayar, A.I.; Nawawi, Z.; Sidik, M.A.B.; Jambak, M.I. Evaluation and Mitigation of Underground Gas Pipeline Coating Stress Due to Nearby Lightning Stroke. In Proceedings of the 2017 International Conference on Electrical Engineering and Computer Science (ICECOS), Palembang, Indonesia, 22–23 August 2017; pp. 275–279. [CrossRef]
25. Wang, X.; Wang, Y.; Sun, T.; Yang, X.; Yang, L.; Qi, Y. Study of Transmission Line AC Interference with Steel-Buried Pipelines under Lightning Strikes. *Electr. Power Syst. Res.* **2023**, *218*, 109226. [CrossRef]
26. El Gayar, A.I.; Abdul-Malek, Z. Induced Voltages on a Gas Pipeline Due to Lightning Strikes on Nearby Overhead Transmission Line. *Int. J. Electr. Comput. Eng.* **2016**, *6*, 495–503. [CrossRef]
27. Rabbani, M.; Oo, A.M.T.; Ahmed, M.R.; Kabir, M.J. Analysis of Lightning Induced Effects on Buried Pipeline Due to Direct Strike on Ground. In Proceedings of the 2016 Australasian Universities Power Engineering Conference (AUPEC), Brisbane, QLD, Australia, 25–28 September 2016; pp. 1–5. [CrossRef]
28. Dushimimana, G.; Simiyu, P.; Ndayishimiye, V.; Niringiyimana, E.; Bikorimana, S. Induced Electromagnetic Field on Underground Metal Pipelines Running Parallel to Nearby High Voltage AC Power Lines. *E3S Web Conf.* **2019**, *107*, 02004. [CrossRef]
29. Southey, R.; Ruan, W.; Dawalibi, F.P.; Fortin, S. Estimating AC Mitigation Requirements for Pipelines Installed in High Voltage AC Corridors: Fault Conditions. In Proceedings of the CORROSION 2003, San Diego, CA, USA, 16–20 March 2003.
30. Christoforidis, G.C.; Labridis, D.P.; Dokopoulos, P.S. Inductive Interference Calculation on Imperfect Coated Pipelines Due to Nearby Faulted Parallel Transmission Lines. *Electr. Power Syst. Res.* **2003**, *66*, 139–148. [CrossRef]
31. Dnv, G.L. *Criteria for Pipelines Co-Existing with Electric Power Lines*; Final Report No. 2015-04; The INGAA Foundation: Washington, DC, USA, 2015.
32. *GB/T 50698-2011*; Standard for AC Interference Mitigation of Buried Steel Pipelines. China Planning Press: Beijing, China, 2011.
33. *GB 6830-1986*; The Tolerable Limits of Danger on Telecommunication Lines from Power Lines. State Bureau of Standards: Beijing, China, 1986.
34. *DL/T 5033-2006*; The Design Rules of Telecommunication Lines Against Danger and Interference Effects from Power Transmission Lines. China Electric Power Press: Beijing, China, 2006.
35. *GB/T 23257-2017*; Polyethylene Coating for Buried Steel Pipeline. Standards Press of China: Beijing, China, 2017.

Disclaimer/Publisher's Note: The statements, opinions and data contained in all publications are solely those of the individual author(s) and contributor(s) and not of MDPI and/or the editor(s). MDPI and/or the editor(s) disclaim responsibility for any injury to people or property resulting from any ideas, methods, instructions or products referred to in the content.